Cooperative Processes Governing Formation of Small Pentanuclear Lanthanide(III) Nanoclusters and Energy Transport within and between Them†

Marlon K. Thompson,‡ Mitko Vuchkov,‖ and Ishenkumba A. Kahwa*,‡

Department of Chemistry and International Centre for Environmental and Nuclear Sciences, University of the West Indies Mona Campus, Kingston 7, Jamaica, West Indies

Received March 5, 2001

Syntheses, lanthanide quantitative analyses, mass spectrometry and luminescence spectroscopy, and decay dynamics of crystals containing pentanuclear hetero-lanthanide(III) nanoclusters $[(Ln'_{5-x}Ln_x)(NO_3)_6(\mu_5\text{-}OH)(\mu_4\text{-}\mathbf{L})_2]$ ($0 \leq x \leq 5$), Ln′ = Eu or Tb; Ln = La−Nd, Sm−Ho (hereafter $Ln'_{5-x}Ln_x$) were undertaken in search of information on factors governing self-assembly processes by which the clusters are formed and electronic interactions within and between them. The data obtained are consistent with the self-assembly of $Ln'_{5-x}Ln_x$ nanoclusters being a concerted process featuring a profound expression of complementarity among mutually bridging $[Ln(\mu_4\text{-}\mathbf{L}]^-$ and $[Ln(NO_3)_2]^+$ components. The energy transport regime in crystals of $Eu_{5-x}Ln_x$ is in the dynamic regime when $x = 0$ or Ln = La and, at 293 K, Ln = Dy, despite the presence of two crystallographically different Eu^{3+} coordination environments which give rise to a doublet in the excitation and emission spectra of $Eu^{3+}(^5D_0)$. The luminescence decay behavior of $Eu^{3+}(^5D_0)$ in $Eu_{5-x}Ln_x$ (Ln = Dy (for 77 K), Sm) is intermediate between the static and dynamic limits and reveals extensive electronic coupling among lanthanide ions, including many-body processes at relatively high Dy^{3+} or Sm^{3+} concentrations.

Introduction

There is considerable interest in the preparation and characterization of materials with molecular or ionic aggregates of nanometer dimensions because of their novelty and potential applications of unusual electronic, catalytic, magnetic, and optical behavior, believed to be peculiar to matter in such dimensions.[1−6] Compounds in which metal ions are "glued" together to produce clusters of nanometer dimensions are particularly interesting because it may be possible to chemically tune their behavior through manipulation of cluster metal compositions. This may in turn result in novel tunable cooperative behavior dependent on intra- and intercluster metal−metal interactions. For example, luminescence properties of europium(III) and terbium(III) ions are readily influenced by their neighbors. [7] Thus, characteristics of terbium(III) and europium(III) nanoclusters such as luminescence lifetimes and intensities might be readily tuned[8] by careful choice of other metal ions with which they share a nanocluster. This feature, when considered in conjunction with the convenience of time-resolved luminescence spectroscopy,[9] the imaging versatility of confocal microscopy,[9] and the emerging potential of quantum dot phenomena, [10] raises prospects of luminescent nanodevices of interest to imaging and diagnostic applications. [9] Similar interest in gadolinium(III) nanoclusters with tunable electron relaxation behavior that may result in tunable cellular water proton relaxation effects can be envisaged for magnetic resonance imaging applications. [11] What is now important in exploring these possibilities is that metallo-nanoclusters be prepared and systematically studied to determine their cooperative electronic properties and the extent and form in which these properties can be manipulated through choice of constituent metals and the nature of the "glue" holding them together. In particular when heterometallic nanoclusters are desired, the processes by which different metal ions are put together (depending on their chemistry and contribution to the energy of the cluster or crystal) to produce heterometallic nanoclusters require better understanding. The chemistry of lanthanide(III) ions is known to

† Dedicated to Professor Kenneth Magnus for his many contributions to the University of the West Indies, especially the Applied Chemistry Program.

* Corresponding author. E-mail: ikahwa@uwimona.edu.jm. Fax: (876) 977-1835. Tel: (876) 927-1910.

‡ Department of Chemistry.

‖ International Centre for Environmental and Nuclear Sciences.

(1) See numerous articles in *Acc. Chem. Res*. **1999**, *32(5)*, Special Issue on Nanoscale Materials, Heath J. R., Guest Editor.

(2) Schmid, G.; Bäumle, M.; Geerkens, M.; Heim, I.; Osemann, C.; Sawitowski, T. *Chem. Soc. Rev.* **1999**, *3*, 179.

(3) Rao, C. N. R.; Kulkarni, G. U.; Thomas, P. J.; Edwards, P. P. *Chem. Soc. Rev.* **2000**, *1*, 27.

(4) Reynolds, C. H.; Annan, N.; Beshah, K.; Huber, J. H.; Shaber, S. H.; Lenkinski, R. E.; Wortman, J. A. *J. Am. Chem. Soc.* **2000**, *122*; 8940.

(5) Chen, S. *J. Am. Chem. Soc.* **2000**, *122*, 7420 and References therein.

(6) Guo, L.; Yang, S. H.; Yang, C. L.; Wang, J. N.; Ge, W. K.; Wong, G. K.L. *Appl. Phys. Lett*. **2000**, *76*, 2901. Guo, L.; Yang, S.; Yang, C.; Wang, J.; Ge, W.; Wong, G. K. L. *Chem. Mater*. **2000**, *12*, 2268.

(7) Kahwa, I. A.; Parkes, C. C.; McPherson, G. L. *Phys. Rev*. **1995**, B52, 1177 Richardson, F. S. *Chem. Rev.* **1982**, *82*, 541. Horrocks, W. deW., Jr.; Sudnick. D. R. *Acc. Chem. Res.* **1981**, *14*, 384. Piguet, C.; Bünzli, J.-C. G.; Bernardinelli, G.; Hopfgartner, G. Petoud, S.; Shaad, O. *J. Am. Chem. Soc*. **1996**, *118*, 6681. Gunnlaugsson, T.; MacDónail, D. A.; Parker, D. *Chem. Commun*. **2000**, 93.

(8) Matthews, K. D.; Fairman, R. A.; Johnson, A.; Spence, K. V. N.; Kahwa, I. A.; McPherson, G. L.; Robotham, H. *J. Chem. Soc., Dalton Trans.* **1993**, 1719.

(9) Good reviews on these subjects can be found in: (a) *Topics in Fluorescence Spectroscopy*; Lakowicz, J. R., Ed.; Plenum Press: New York, 1991−1994; Vol. 1−4. (b) Lakowicz, J. R. *Principles of Fluorescence Spectroscopy*, 2nd ed.; Kluwer Academic/Plenum Publishers: New York, 1999. (c) *Fluorescence Microscopy and Fluorescent Probes*; Slavík, J., Ed.; Plenum Press: New York, 1996

(10) Nirmal, M.; Brus, L. *Acc. Chem. Res*. **1999**, *32*, 407. Michler, P.; Imamoglu, A.; Mason, M. D.; Carson, P. J.; Strouse, G. F.; Buratto, S. K. *Nature* **2000**, *406*, 968.

(11) Laufer, R. B. *Chem. Rev*. **1987**, *87*, 901; Li, W.-H.; Fraser, S. E.; Thomas J. Meade, T. J. *J. Am. Chem. Soc*. **1999**, *121*, 1413; Caravan, P.; Ellison, J. J.; McMurry, T. J.; Laufer, R. B. *Chem. Rev*. **1999**, *99*, 2293.

10.1021/ic0102440 CCC: $20.00
Published on Web 07/10/2001

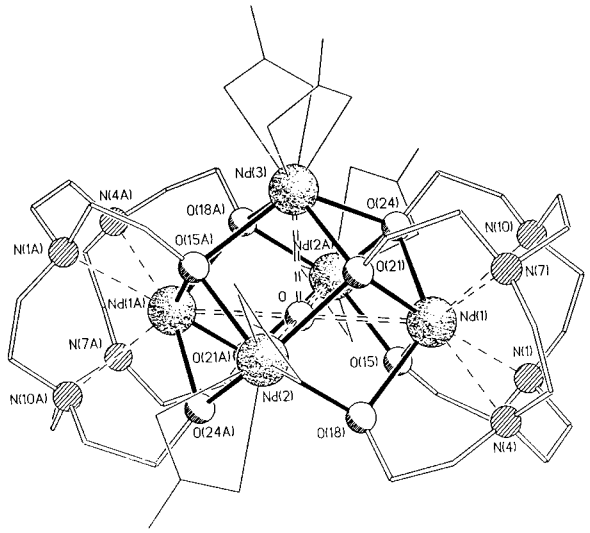

Figure 1. The molecular structure of the pentaneodymium(III) nanocluster Nd_5, i.e., $[\{Nd(NO_3)_2\}3(\mu_5\text{-OH})(Nd(\mu_4\text{-}\mathbf{L}))_2]$. The "OH glue" is O at the center and nitrate groups are shown as thin lines at Nd(2), Nd(2A), and Nd(3).

depend almost exclusively on their ionic potentials, which increase systematically from lanthanum(III) to lutetium(III). [12] Nanoclusters of lanthanide(III) ions are thus among the simplest systems with the potential to reveal systematic information on metal−metal cooperative chemistry governing formation of heterometallic nanoclusters. Further, the relative simplicity of the luminescence spectra of europium(III)[13] makes it a good probe for the outcome of the cooperative metal−metal activity.

For these reasons, we have prepared and explored the chemical and electronic behavior of hetero-pentanuclear complexes of luminescent europium(III) and terbium(III) ions, $[(Ln'(NO_3)_2)_3(\mu_5\text{-OH})(Ln(\mu_4\text{-}\mathbf{L}))_2]_{(s)}$ (hereafter Ln'_5, Ln′ = Eu, Tb), featuring small molecular nanoclusters (molecular diameter, ca. 1.2 nm) with five rare earth atoms built (in C_{4v} symmetry) around an μ_5-OH "glue". Structural details are a subject of another extensive submission; [14] thus, only a summary is given here to facilitate clarity of this presentation.

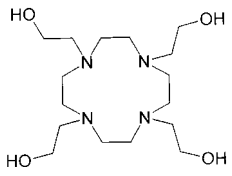

$H_4\mathbf{L}$

A representative molecular structure, that of $[(Nd(NO_3)_2)_3(\mu_5\text{-OH})(Nd(\mu_4\text{-}\mathbf{L}))_2]$ (hereafter Nd_5) at 110 and 293 K (Figure 1), shows that members of the family of lanthanide(III) pentanuclear nanoclusters $[(Ln(NO_3)_2)_3(\mu_5\text{-OH})(Ln(\mu_4\text{-}\mathbf{L}))_2]$ (herein after Ln_5, Ln = Pr, Nd, Sm−Ho), have two principal metal ion environments. In one case (hereinafter **Site 1**) a lanthanide(III) ion (Nd(1) and Nd(1A)) is encapsulated in the macrocyclic chelate $\mathbf{L}^{4-}$, where it is bound to four tertiary amines and associated four alkoxides, and completes a 9-fold coordination polyhedron of C_{4v} symmetry (Figure 2) by bonding to the μ_5-OH^- "glue". In another case (hereinafter **Site 2**), the lanthanide(III) ion binds two bidentate nitrato ligands and the μ_5-OH^- "glue" and completes a distorted tricapped trigonal prismatic coordination polyhedron (Figure 3) of at most C_3 symmetry by bridging to two of the alkoxide sites on each $\mathbf{L}^{4-}$ chelate. However, within this **Site 2** category there are two slightly different Ln^{3+} environments; one is in the equatorial (Nd(2) and Nd(2A)) and the other is in the polar (Nd(3)) position of the square pyramidal arrangement of the five Ln atoms (Figure 1). The critical difference between the Nd(2) and Nd(3) positions is that the Nd(3) site forms multiple bridges with all four other lanthanide(III) ions in the nanocluster while the Nd(2) and Nd(2A) sites are so bridged to only three other Ln^{3+} ions. When the Ln−O−Ln bridges become crucial conduits of electronic interactions[13] within the Ln_5 nanoclusters (e.g., via through bond, exchange or superexchange electronic interactions) then site Nd(3) could be more efficient than Nd(2) at redistributing electronic energy. The differences between sites Nd(1), Nd(2), and Nd(3) notwithstanding, the most exciting feature of the Ln_5 nanoclusters is that the μ_5-OH^- "glue" which links all five lanthanide ions together might effectively couple these ions and cause the nanocluster to operate as one unique entity whose electronic behavior is determined by the nature and strength of coupling among the clustered Ln^{3+} ions.

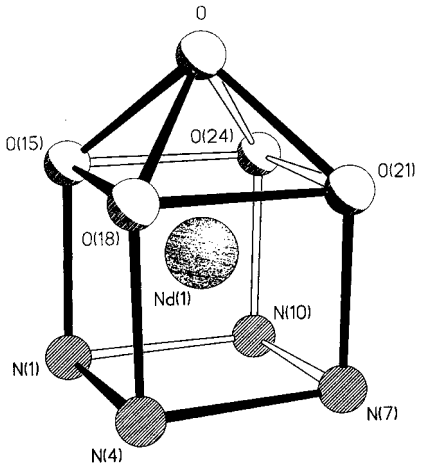

Figure 2. The ca. C_4v coordination polyhedron around Nd1 (**Site 1**).

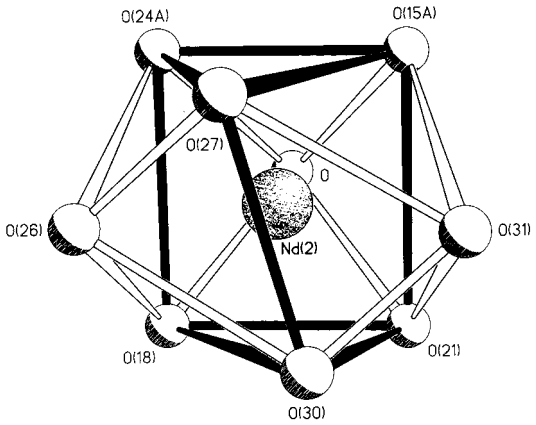

Figure 3. The distorted tricapped trigonal primatic coordination polyhedron of Nd_2 (**Site 2**). The environment of Nd_3 is similar.

(12) Kahwa, I. A. *J. Therm. Anal.* **1982**, *25*, 525.
(13) (a) Försberg, J. H., *Coord. Chem. Rev.* **1973**, *10*, 195. (b) Sinha, S. P.; Butter, E. Mol. Phys. **1969**, *16*, 285. (c) Gajadhar−Plummer, A. S.; Kahwa, I. A.; White, A. J. P.; Williams, D. J. *Inorg. Chem.* **1999**, *38*, 1745. (d) Supkowski, R. M.; Horrocks, W. deW., Jr. *Inorg. Chem.* **1999**, *38*, 5616. Lessmann, J. L.; Horrocks, W. deW., Jr. *Inorg. Chem.* **2000**, *39*, 3114. Epstein, D. M.; Chappell, L. L.; Khalili, H.; Supkowski, R. M.; Horrocks, W. deW., Jr.; Morrow, J. R. *Inorg. Chem.* **2000**, *39*, 2130. Choppin, G. R.; Peterman, D. R. *Coord. Chem. Rev.* **1998**, *174*, 283.
(14) Thompson, M. K.; Kahwa, I. A.; Lough, A.; White, A. J. P.; Williams, D. J. Manuscript in preparation.

Intracluster short Nd−O−Nd separations are within 3.7−3.8 Å while the shortest intercluster Nd···Nd distance is ca. 9.33 Å. For a luminescent Ln^{3+} ion, the ratio of intra- to intercluster Ln−Ln energy transfer rates by the common through space Dexter−Förster dipolar mechanisms (transfer rate $k = C/R^6$, C = dipolar coupling constant, and R = Ln−Ln separation)[15] is up to roughly 260:1. Further, if superexchange, exchange, and through bond Ln−Ln intracluster electronic interactions become significant, this ratio could be much higher thereby readily allowing the distinct behavior of the individual pentanuclear nanoclusters to be observed and studied by luminescence decay dynamical techniques. We were thus interested in the preparation and luminescence characteristics of homo-lanthanide(III) pentanuclear nanoclusters, Eu_5 and Tb_5, and their hetero-lanthanide-(III) pentanuclear derivatives, $[(Ln'_{5-x}Ln_x)(NO_3)_6(\mu_5\text{-OH})(\mu_4\text{-}\mathbf{L})_2]$, (herein after $Ln'_{5-x}Ln_x$, Ln′ = Eu or Tb and Ln = La − Nd, Sm−Ho but not Pm, Eu or Tb). It was hoped that detailed investigations would reveal the chemistry and electronic behavior of lanthanide(III) ions in **Site 1** and **Site 2** thereby providing clues on factors governing aggregation processes through which the homo- and hetero-lanthanide nanoclusters self-assemble as well as cooperative electronic behavior within and between them. Herein we report on the competitive lanthanide(III) complexation behavior of hetero-lanthanide(III) nanoclusters, $Eu_{5-x}Ln_x$ ($0 \le x \le 5$)), and their luminescence characteristics and intracluster and intercluster electronic interactions.

Experimental Section

Materials. Lanthanide(III) nitrates were obtained by neutralizing corresponding oxides (Aldrich; at least 99.99% purity) with concentrated nitric acid, followed by evaporation to near dryness. 1-Aziridineethanol (Aldrich) was of 97% purity inhibited with 1−3% dissolved sodium hydroxide.

Spectral and Quantitative Analyses. Fast Atom Bombardment mass spectra (FAB MS) (with *m*-nitrobenzyl alcohol matrix) were obtained using a Concept mass spectrometer at Cambridge University or VG Masslab Trio-2 at the University of Miami. Isotopic abundance patterns were calculated using the Sheffield ChemPuter Isotope Patterns Calculator from Sheffield University, UK, which is accessible on the Internet at: http://www.shef.ac.uk/chemistry/chemputer/isotopes.html. Carbon−hydrogen−nitrogen analyses were done at MEDAC Ltd., Surrey, UK. Lanthanide concentrations were determined by Energy-Dispersive X-ray Fluorescence Spectroscopy[16a] (EDXRF) using a Kevex EDX-771 at the International Center for Environmental and Nuclear Sciences, University of the West Indies, Jamaica. The Kevex EDX-771 EDXRF spectrometer is equipped with a liquid nitrogen cooled Si(Li) detector (0.3 mil Be window) and a 60 KV, 3 mA (maximum) Rh anode X-ray tube. Measurement and data reduction software is executed on a Dell 486/D50 personal computer that automates spectrometer parameters and sample tray position. Standards and unknown thin-film samples (25-mm diameter) were assembled in a 16-position sample tray with the "spot side down" on a clean dust-free area. The lanthanide elements of interest were measured using Ge-secondary target, which allows simultaneous excitation of their characteristic $L_{\alpha,\beta}$ lines. The X-ray tube was operated at 20.0 KV and 2.2 mA. Each sample was irradiated and counted for 300 s. The "thin-film" methodology for quantitative XRF analysis[16b] was used. Twenty-five cm^3 of each sample was spiked on 25-mm Whatmann filter papers and dried under an UV lamp at low power for 15 min. One of every 10 samples was spiked in triplicate to check sample preparation variability. Linear calibration curves were obtained for lanthanide analytes using single element standard solid samples provided by Micromatter, Inc., Deer Harbor, WA, and single element stock solutions spiked on filter paper. A multi-element standard solution was used to check the accuracy of the single element calibration curves. A set of 15 samples were analyzed by Neutron Activation Analyses (NAA)[17] and agreement with EDXRF analyses was better than 5%.

The luminescence and excitation spectra were recorded using a Yvon Jobin FluoroMax-2 Spectrofluorometer with samples sealed in glass tubes. Luminescence decay curves were acquired using either a Continuum ND6000 dye laser pumped by a Continuum Powerlite 8000 Nd/YAG laser or a Photon Technology International PL201 dye laser pumped by a matching PL2300 nitrogen laser as described previously.[13c] Selective excitation for $Eu^{3+}(^5D_0)$ was achieved using a Rhodamine6G dye tuned at either 578 or 579 nm.

Preparation of Polycrystalline $Ln'_{5-x}Ln_x$ (Ln = La−Nd, Sm−Ho but not Pm, Eu or Tb; Ln′ = Eu or Tb). A desired mixture of $Ln(NO_3)_3.nH_2O$ and $Ln'(NO_3)_3.nH_2O$ salts giving a total of one mmol of lanthanide(III) ions in 50 cm^3 of anhydrous ethanol was added dropwise over 24 h to a refluxing solution of 2.5 mmol of 1-aziridineethanol in 150 cm^3 anhydrous ethanol resulting in a cloudy solution. Reflux was maintained and formation of cube- or needlelike crystals of $Ln'_{5-x}Ln_x$ was achieved within 2 days at yields of ca. 30−99% (depending on the nature of hetero-lanthanide(III) ions used).

Results and Discussion

Preparation and Characterization of Complexes. The products containing La, Pr, and Nd featured the same crystal morphology (cubes) as that of Nd_5, the room (293 K) and low (110 K) temperature crystal and molecular structures of which have been established.[14] The products containing Ce, Sm−Ho featured the same crystal morphology (needles) as that of the analogous homo-pentanuclear samples. Indeed preliminary single-crystal X-ray analyses of the La_4Eu_6 hetero-pentanuclear mixed metal complex confirmed that the complex has the same unit cell symmetry as that of Nd_5. Also, FAB MS (Figure 4) feature pentanuclear ($[\{Ln(NO_3)_2\}_2Ln(O)(Ln(\mu_4\text{-}\mathbf{L}))_2]^+$) and tetranuclear ($[\{Ln(NO_3)_2\}_2(\mu_5\text{-OH})(Ln(\mu_4\text{-}\mathbf{L}))_2]^+$) clusters in support of a pentanuclear structural motif for the Ln_5 (Ln = Pr and Ho) complexes. Pentanuclear nanoclusters lose $2(NO_3)$ and $Ln(NO_3)_4$ units to produce pentanuclear and tetranuclear species, ($[\{Ln(NO_3)_2\}_2Ln(O)(Ln(\mu_4\text{-}\mathbf{L}))_2]^+$) and ($[\{Ln(NO_3)_2\}_2(\mu_5\text{-OH})(Ln(\mu_4\text{-}\mathbf{L}))_2]^+$), respectively. Similar fragmentation patterns are observed for pentanuclear complexes of Ln^{3+} with Ln = Nd, Eu, and Y. For these reasons, all complexes Ln_5 (Ln = Pr, Nd, Sm−Ho) and their mixed metal analogues were considered to be of the same pentanuclear molecular structure. For mixed-metal samples, Energy Dispersive X-ray fluorescence (EDXRF) or Neutron Activation Analyses (NAA) techniques were used to establish the concentrations of the lanthanide elements (see Experimental Section). First, we examine competitive complexation events in which lanthanide(III) ions of different sizes are selected from reaction mixtures for incorporation into crystalline products of $Ln'_{5-x}Ln_x$ hetero-lanthanide(III) nanoclusters.

Competitive Complexation of Ln^{3+} and Ln'^{3+} ions in $Ln'_{5-x}Ln_x$ ($x = 1-5$) Nanoclusters. To obtain comparative information on relative lanthanide(III) ion selectivity of the $Eu_{5-x}Ln_x$ and $Tb_{5-x}Ln_x$ systems (Ln = La − Nd, Sm−Ho) we studied the lanthanide content of crystals obtained from refluxing solutions which initially contained equimolar amounts of the probe ions, Eu^{3+} or Tb^{3+}, and hetero-lanthanide(III) ions (Ln^{3+}). The amounts of the probe europium(III) or terbium(III) ions incorporated in the crystalline products were found to increase

(15) Dexter, D. L. *J. Chem. Phys.* **1953**, *21*, 836. Förster, T. *Z. Naturforch.* **1949**, 49, 321.

(16) (a) Johnson, A.; Lalor, G. C.; Robotham, H.; Vutchkov, M. K. *J. Radioanal. Nucl. Chem.* **1996b**, *209*, 101. (b) Jenkins, R.; Gould, R. W.; Gedcke, D. *Quantitative X-ray Spectrometry*; Marcel Dekker: New York, 1991.

(17) Grant, C.; Lalor, G. C.; Preston, J.; Rattray, R.; Vutchkov, M. *Jamaican J. Sci. Technol.* **1998**, *9*, 63. Vutchkov, M.; Grant, C.; G. C. Lalor, G. C.; Preston, J. *J. Radioanal. Nucl. Chem.* **2000,** *224*, 355.

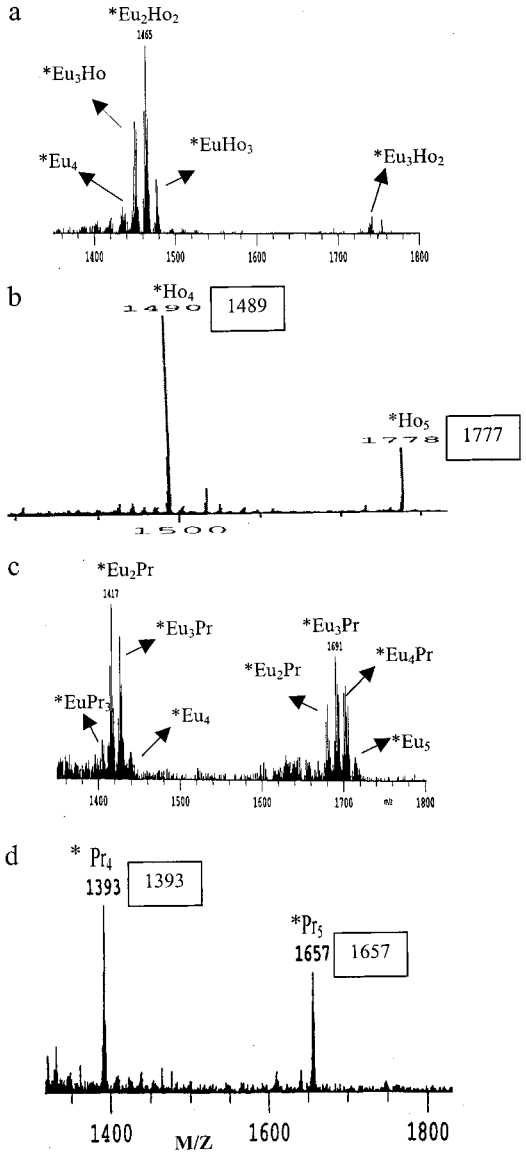

Figure 4. Partial FAB MS and LSIMS of $Eu_{5-x}Ln_x$. (a) Ln = Ho, $x = 1.55$; (b) Ln = Ho, $x = 5$; (c) Ln = Pr, $x = 1.25$; (d) Ln = Pr, $x = 5$. Peak assignments are indicated by the order of clustering. General stoichiometries of homo-lanthanide fragments are as follows: $*Ln_5 = [Ln_5(NO_3)_4(O)(\mu_4\text{-}\mathbf{L})_2]^+$; $*Ln_4 = [Ln_4(NO_3)_2(\mu_5\text{-}OH)(\mu_4\text{-}\mathbf{L})_2]^+$. Calculated *m*/*z* values appear in rectangular boxes besides observed ones for spectra (b) and (d). Hetero-lanthanide clusters are similar except that the order of clustering is derived from the sum of atoms of the hetero-lanthanide elements.

with increasing cation radii difference $\Delta r = r_{Ln} - r_{Ln'}$ (Figure 5). For comparative purposes, ionic radii for coordination number 6 (r) are used throughout this presentation.[18] We thus conclude that, on the average, crystals of $Eu_{5-x}Ln_x$ and $Tb_{5-x}Ln_x$ nanoclusters (Ln = La − Nd, Sm−Ho) favor the smaller of two cations competing for incorporation into crystalline products. It is noteworthy that the largest lanthanide(III) ions Ln^{3+} (Ln = La, Ce) do not form homo-pentanuclucear Ln_5 complexes, but the smaller Eu^{3+} and Tb^{3+} ions seem to exert a stabilizing influence. Hence corresponding mixed-metal pentanuclear complexes, $Eu_{5-x}Ln_x$ and $Tb_{5-x}Ln_x$ (Ln = La, Ce), are readily formed even though the pure La_5 and Ce_5 homo-pentanuclear compounds are not observed. This preference for small lanthanide(III) ions is also evident in the slopes of the plots (Figure

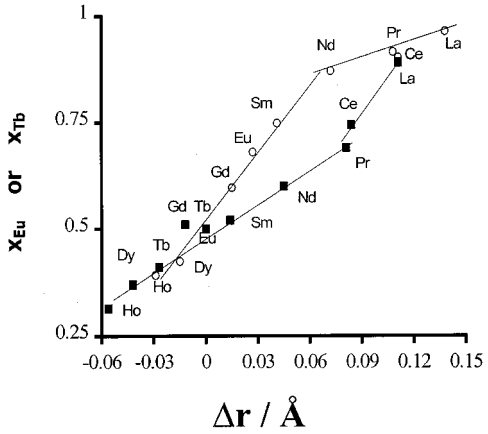

Figure 5. The dependence of Eu^{3+} (x_{Eu}) and Tb^{3+} (x_{Tb}) mole fractions found in the crystalline hetero-lanthanide $Ln'_{5-x}Ln_x$ (Ln′ = Eu or Tb; Ln = lanthanide element) products on the ionic radii difference, $\Delta r = r_{Ln} - r_{Ln'}$, for Ln^{3+} and Ln'^{3+}. O = the $Tb_{5-x}Ln_x$ series; ■ = the $Eu_{5-x}Ln_x$ series.

5) where, consistent with the smaller size of Tb^{3+} compared to that of Eu^{3+}, the slope of the $Tb_{5-x}Ln_x$ system is steeper. The changes in slopes at Ln = Pr reflect changes in chemistry; for the $Eu_{5-x}Ln_x$ system, for which introduction of larger ions such as Ce^{3+} or La^{3+} is most destabilizing, the corresponding slope is much steeper (ca. two times) than the one corresponding to Ln^{3+} (Ln = Ho−Nd). This is an indication that a higher concentration of Eu^{3+} ions in europium(III)−cerium(III) ($Eu_{5-x}Ce_x$) and europium(III)−lanthanum(III) ($Eu_{5-x}Ln_x$) hetero-lanthanide nanoclusters is needed to achieve their stability. The diminished slope of the $Tb_{5-x}Ln_x$ system for Ln = Nd, Pr, Ce, La is curious, but could not be expected to be too large because the mole fraction (over 0.85 at Ln = Nd) of Tb^{3+} ions required to achieve stability of these mixed metal complexes is already too high (Figure 5).

The results in Figure 5 suggest that the formation of $Eu_{5-x}Ln_x$ and $Tb_{5-x}Ln_x$ complexes may involve metal−metal cooperative processes in which the relative stabilities of individual pentanuclear nanoaggregates play prominent roles. We explored this possibility in more detail using europium(III) crystalline products, $Eu_{5-x}Ln_x$ (Ln = Sm, Tb or Dy), isolated from mother liquors with a wide range of initial Ln^{3+} and Eu^{3+} concentrations. In this case, the more useful comparative parameter is the cation selectivity index (I_D) (eq 1), which was developed earlier[8,13c,19] to extract information on competitive complexation events by comparing the initial metal ion concentrations of mother liquors with those found in crystalline products:

$$I_D(X_{Ln})/(X_{Eu}) + 1 = 1/x_{Eu} \qquad (1)$$

I_D is a ratio of the probability of incorporating the hetero-cation Ln^{3+} (P_{Ln}) into the crystalline products relative to that of Eu^{3+} (P_{Eu}), i.e., $I_D = P_{Ln}/P_{Eu}$. (X_{Ln}) and (X_{Eu}) are respectively the relative initial mole fractions of the hetero-lanthanide(III) ions and Eu^{3+} in the parent reaction mixture; x_{Eu} is the relative mole fraction of Eu^{3+} found in the $Eu_{5-x}Ln_x$ crystalline products. For comparative purposes, relative mole fractions are restricted to total lanthanide contents only. As shown in Figure 6 (insert C), analyses of the samarium and europium content of crystalline $Eu_{5-x}Sm_x$ products reveals a cation selectivity index, $I_D = 0.77$ which shows that the smaller europium(III) ions ($r = 0.95$ Å) are preferred over the slightly larger samarium(III) ions ($r =$

(18) Shannon, R. D.; Prewitt, C. *Acta Crystallogr*. **1971**, *B25*, 525.

(19) Howell, R. C.; Spence, K. V. N.; Kahwa, I. A.; White, A. J. P.; Williams, D. J. *J. Chem. Soc., Dalton Trans*. **1996**, 961

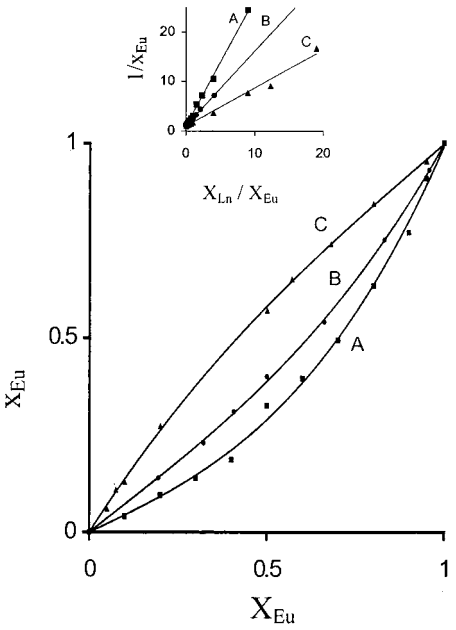

Figure 6. The dependence of the mole fraction (x_{Eu}) of Eu^{3+} in the crystalline hetero-lanthanide $Eu_{5-x}Ln_x$ products on the initial mole fraction (X_{Eu}) in the parent reaction mixture (A, Ln = Dy; B, Ln = Tb; C, Ln = Sm). The curves are best fit on a quadratic equation: $x_{eu} = \alpha(X_{Eu})^2 + \beta(X_{Eu})$ where $\alpha = 0.77$, 0.41, and -0.338 and $\beta = 0.20$, 0.58, and 1.33 for curves A, B, and C, respectively. The corresponding cation discrimination indices derived from linear plots in the insert are 2.58, 1.51, and 0.77 for A, B and C, respectively.

0.964 Å) for incorporation into crystalline aggregates of $Eu_{5-x}Sm_x$ nanoclusters. By contrast, crystalline $Eu_{5-x}Ln_x$ with Ln = Tb (Figure 6, insert B) and Dy (Figure 6, insert A) feature higher cation selectivity indices of $I_D = 1.51$ and 2.58 favoring respectively the smaller terbium(III) ($r = 0.923$ Å) and dysprosium(III) ($r = 0.908$ Å) ions over, the now larger, europium(III) ion ($r = 0.95$ Å). However, the cation selectivity index (I_D), which is indicative of average behavior, is not specific enough to provide information on the discrimination/selectivity processes governing competitive complexation through which individual nanoclusters are assembled. This is because crystalline hetero-lanthanide(III) products, $Eu_{5-x}Ln_x$, may be built by assembling individual homo-pentanuclear nanoclusters, Eu_5 and Ln_5 only, or a variety of mixed-metal nanoclusters $Eu_{5-x}Ln_x$ ($0 \le x \le 5$). Thus more detailed information on the competitive complexation dynamics among Eu^{3+} and hetero-Ln^{3+} ions was sought directly from the relationship between the relative mole fraction ($x_{(Eu)}$) of europium(III) ions incorporated in the crystalline products $Eu_{5-x}Ln_x$ (Ln = Sm, Tb or Dy) and the relative mole fraction of europium(III) in the parent reaction mixture ($X_{(Eu)}$) (Figure 6). There is no complexation competition when homo-metallic nanoclusters Eu_5 and Ln_5 are being built, hence the attendant processes are expected to depend on the availability of the respective metal ions (i.e., X_u) for Eu_5 in the mother liquor. On the other hand, formation of hetero-lanthanide nanoclusters, $Eu_{5-x}Ln_x$ ($0 < x < 5$), requires availability and participation of both Eu^{3+} and Ln^{3+} ions, hence their formation probability should be a product of the mole fractions of europium (X_{Eu}) and the hetero-lanthanide ($(1 - (X_{Eu}))$ in the mother liquor as: $(X_{Eu})(1 - (X_{Eu}))$. Hence, the total europium content in the crystals (x_{eu}) is expected to be proportional to the sum of the contributions of homo- and hetero-lanthanide clusters i.e., $(X_{Eu})(1 - (X_{Eu})) + (X_{Eu})$, which reduces to a quadratic equation after work up. Indeed, in all three cases (Figure 6) the data are best described by such a quadratic relationship, in the simpler form:

$$x_{eu} = \alpha(X_{Eu})^2 + \beta(X_{Eu}) \qquad (2)$$

Where α = an average interaction parameter leading to the formation of hetero-lanthanide nanoclusters while β serves a similar purpose for homo-lanthanide nanoclusters. This means that the crystalline $Eu_{5-x}Ln_x$ (Ln = Sm, Tb or Dy) products comprise both homo-lanthanide(III) and hetero-lanthanide(III) nanoclusters (i.e., all $Eu_{5-x}Ln_x$ ($0 \le x \le 5$)). For $Eu_{5-x}Sm_x$ nanoclusters (with $I_D < 1$) samarium−europium cooperative activity, which couples favored europium(III) and less favored samarium(III) cations, is essentially detrimental to the up-take of europium(III) ions into crystalline $Eu_{5-x}Sm_x$ products. Thus, homo-pentanuclear Eu_5 nanoclusters are expected to be the dominant species. Accordingly, the coefficient α (eq 2 and Figure 6, C) is negative for $Eu_{5-x}Sm_x$ because europium−samarium hetero-nuclear nanoclusters are discriminated against while β is relatively large because incorporation of homo-pentanuclear Eu_5 nanoclusters into crystalline $Eu_{5-x}Sm_x$ products is preferred. By contrast, crystalline $Eu_{5-x}Ln_x$ (Ln = Tb (Figure 6B) and Dy (Figure 6, A)) products (with $I_D > 1$), which favor the smaller Tb^{3+} and Dy^{3+} over Eu^{3+}, feature positive and much larger α coefficients than found for $Eu_{5-x}Sm_x$ (Figure 6). In the context of eq 2, this is because of the more significant contribution of hetero-lanthanide $Eu_{5-x}Ln_x$ ($0 < x < 5$) nanoclusters to the population of Eu^{3+} ions in those crystalline $Eu_{5-x}Ln_x$ products. Accordingly, the corresponding β coefficients are smaller, because of the diminished contribution of Eu_5 nanoclusters to the population of Eu^{3+} ions. We have examined data from previous lanthanide(III) ion competitive complexation studies[8,13c,19] and found eq 2 to be a satisfactory general description of the relationship between the lanthanide-(III) ion concentrations in mother liquors and the dinuclear crystalline complexes recovered therefrom.

Whereas the above results have established the presence of hetero-lanthanide(III) nanoclusters in crystalline $Eu_{5-x}Ln_x$, the nature of those nanoclusters is not inferable from eq 2. This is because a variety of hetero-lanthanide(III) nanoclusters $Eu_{5-x}Ln_x$ ($x = 1-4$) may be used to build the crystalline products. But if cluster or crystal formation proceeds under highly selective thermodynamic or kinetic circumstances the population of one or only some out of the six possible nanoclusters $Eu_{5-x}Ln_x$ ($x = 0-5$) may dominate. It is also important to note that the most favored metal ions for inclusion in crystalline $Eu_{5-x}Ln_x$ will be depleted from the mother liquor at a faster rate than the less favored ones. Since $[Ln\mathbf{L}]^-$ complexes are kinetically very stable (dissociation constant $k = 10^{-7} - 10^{-6}$ s^{-1})[20] against dissociative processes, kinetic crystalline $Eu_{5-x}Ln_x$ products with heterogeneous single-crystals in which $Ln_{5-x}Eu_x$ ($0 \le x \le 5$) nanoclusters are not uniformly distributed can be expected. Intriguingly, in such cases the nature of the nanocluster formed and its location in the crystal would dependent on the instantaneous composition of the mother liquor.[21] On the other hand, thermodynamic crystalline products with uniform distributions of nanoclusters may dominate if the crystallization process is concerted and dependent on initial conditions, or if there are efficient dynamic mechanisms that correct and update, in real time, the composition of crystalline $Eu_{5-x}Ln_x$ products. While such corrective mechanism are a hallmark of exacting biological processes, limited but important information on their activity

(20) Morrow, J. R.; Chin, K. O. A. *Inorg. Chem.* **1993**, *32*, 3357.
(21) Omary, M. A.; Hall, D. R.; Shankle, E. G.; Siemiaczuk, A.; Patterson, H. H. *J. Phys. Chem. B* **1999**, *103*, 3845.

in abiotic processes has recently been discovered in polymeric polymetallic oxides.[22] These issues are important for clusters because of the very attractive potential for chemical tuning of their magnetic, magnetooptical, optical, electronic, and other properties through processes in which metal ions have to compete for coordination sites. To determine whether crystalline $Eu_{5-x}Ln_x$ products do indeed contain a variety of hetero-lanthanide(III) nanoclusters or one major such species, we obtained FAB MS spectra of several complexes. As seen in Figure 4c the FAB MS of the crystalline $Eu_{5-x}Pr_x$ product does contain a variety of pentanuclear, $[(Eu_{5-x}Pr_x)(NO_3)(\mu_5\text{-OH})(\mu_4\text{-}\mathbf{L})_2]^+$ ($x = 0, 1, 2, 3$), and tetranuclear, $[(Eu_{4-x}Pr_x)(NO_3)_3(\mu_5\text{-OH})(\mu_4\text{-}\mathbf{L})_2]^+$ ($x = 1, 2$), hetero-lanthanide species. There are tetranuclear $[(Eu_{4-x}Ho_x)(NO_3)_3(\mu_5\text{-OH})(\mu_4\text{-}\mathbf{L})_2]^+$ ($x = 1-4$) clusters in the FAB MS of the crystalline $Eu_{5-x}Ho_x$ product (Figure 4a); pentanuclear clusters are also present but with low intensities. Although FAB MS spectral data do not always correspond to species actually present in the solid samples because of recombinations or entirely new reactions in the FAB MS environment, taken together with X-ray structures, the FAB MS data are consistent with the presence of a variety of $Eu_{5-x}Ln_x$ ($0 = x = 5$) nanoclusters, in hetero-lanthanide(III) crystalline products. What now remains is to determine conclusively whether such clusters are indeed present, if they are uniformly distributed in the crystalline products and if the chemistry of **Site 1** and **Site 2** are significantly different.

Luminescence spectroscopy of $Eu^{3+}(^5D_0)$ can provide detailed information on differences in crystal field strengths and symmetry of coordination sites, which are inferable from intensities and multiplicities of $Eu^{3+}(^5D_0 \rightarrow {}^7F_J;\ J = 0-2)$ emissive electronic transitions.[13] Corresponding luminescence decay dynamical behavior can report on proximal metal ions, which quench the $Eu^{3+}(^5D_0 \rightarrow {}^7F_J;\ J = 0-2)$ emission and cause predictable changes in emission decay rates.[7,8,13c,19] For these reasons we studied the luminescence behavior of crystalline $Eu_{5-x}Ln_x$ products in search of more detailed information on the nature of nanoclusters therein (including coordination preferences of **Site 1** and **Site 2**) and insights into the processes which govern their formation as well as their chemical and electronic cooperative activity.

Luminescence Spectroscopy. Illumination of the polycrystalline homopentanuclear Eu_5 complex with 395 nm radiation at 77 or 297 K produces red emission featuring sharp peaks typical of $Eu^{3+}(^5D_0) \rightarrow Eu^{3+}(^7F_J;\ J = 0-4)$ electronic transitions (Figure 7a). The spectral profile is characteristically that of $Eu^{3+}(^5D_0)$ in coordination environments of low symmetry (C_{nv} or lower), [13] which is consistent with the expected low crystal electric field symmetry at both **Site 1** and **Site 2** in Ln_5 (Figures 2 and 3). The most curious features in this emission spectrum are the doublet at 578.3 and 579.2 nm, which correspond to the $Eu^{3+}(^5D_0) \rightarrow Eu^{3+}(^7F_0)$ transition, and the four peaks at ca. 585−597 nm, which correspond to $Eu^{3+}(^5D_0) \rightarrow Eu^{3+}(^7F_1)$ transitions. Since both $^5D_0$ and $^7F_0$ states are singlets, the $Eu^{3+}(^5D_0) \rightarrow Eu^{3+}(^7F_0)$ doublet can only mean that the Eu_5 nanocluster has at least two distinct Eu^{3+} coordination environments with significant differences in symmetry and crystal field strength. The four peaks (and several additional shoulders) in the $Eu^{3+}(^5D_0) \rightarrow Eu^{3+}(^7F_1)$ region (Figure 7a) support this conclusion since each Eu^{3+} environment can give rise to a maximum of three peaks because of the triplet nature of the $Eu^{3+}(^7F_1)$ state. The 77 K excitation spectrum of polycrystalline Eu_5 monitored at 616 nm, shows (Figure 7b) absorption peaks

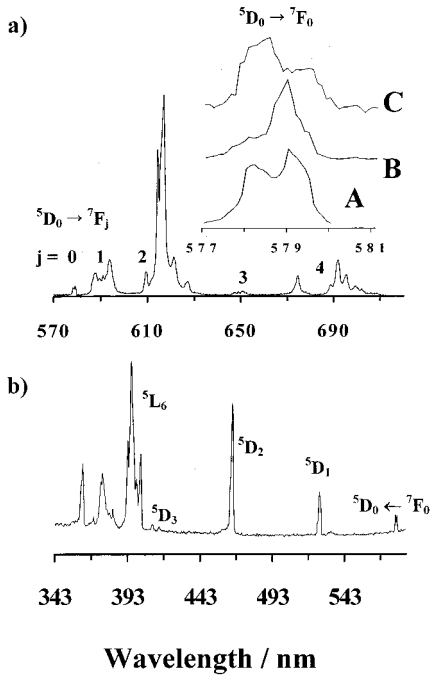

Figure 7. (a) Emission ($\lambda_{exc} = 395$ nm) and (b) excitation ($\lambda_{em} = 616$ nm) spectra of Eu_5 at 77 K. Insert in (a) shows $Eu^{3+}(^5D0 \rightarrow {}^7F_0)$ in Eu_5 (A), Eu_3La_2 (B), and $Eu_{0.70}Tb_{4.30}$ (C).

also typical of Eu^{3+} in low symmetry and again the $Eu^{3+}(^5D_0) \rightarrow Eu^{3+}(^7F_0)$ region features a clear doublet consistent with two significantly different Eu^{3+} environments.

The most obvious source of the doublet behavior in the $Eu^{3+}(^5D_0) \rightarrow Eu^{3+}(^7F_0)$ region of the emission and excitation spectra (Figure 7) are the two different low symmetry Eu^{3+} coordination polyhedra at **Site 1** and **Site 2** in the Eu_5 nanocluster. The nature of coordinating atoms at these sites and their dispositions are different, being C_{4v} for **Site 1** (4 nitrogens and 5 oxygens) and at most C_3 for the highly distorted tricapped trigonal prism at **Site 2** (9 oxygens). Thus the doublet for the $Eu^{3+}(^5D_0) \rightarrow Eu^{3+}(^7F_0)$ transition is due to differences in composition and symmetry of Eu^{3+} coordination polyhedra of **Site 1** and **Site 2**. The possibility of having a mixture of different compounds was eliminated by lifetime measurements which yielded perfect single-exponential decay curves for the emission monitored at 616 nm (vide infra). It was therefore interesting to determine whether the differences in the chemistry of **Site 1** and **Site 2** were large enough to reveal measurable selectivity consistent with the lanthanide contraction.[12] The stability constants of the $Ln^{3+}/\mathbf{L}^{4-}$ system are not known for all lanthanide(III) ions but can be expected to increase with decreasing Ln^{3+} radius in a manner similar to the $Ln^{3+}/\mathbf{DOTA}^{4-}$ or their derivatives.[23] With this consideration we can expect **Site 1**, where the $[Ln\mathbf{L}]^-$ species are located, to be preferred by small lanthanide(III) ions. On the other hand, each pentanuclear nanocluster is built with the aid of several Ln-O-Ln bridges across alkoxide sites of these $[Ln\mathbf{L}]^-$ species. Strong interactions between Ln^{3+} ions (especially small ones) and $\mathbf{L}^{4-}$ can be expected to reduce the Lewis basicity of the alkoxide sites thereby making them poor electron donors for bridging lanthanide(III) ions. This could lead to less stable bridges in the pentanuclear nanoclusters and low stability for the nanoclusters themselves. Therefore in competition for **Site 1** the $[Ln\mathbf{L}]^-$ species of a larger Ln^{3+} ion would in this case be favored, the stability trend of isolated $[Ln\mathbf{L}]^-$ species

(22) Vander Griend, D. A.; Malo, S.; Wang, T. K.; Poeppelmeier, K. R. *J. Am. Chem. Soc.* **2000**, *122*, 7308.

(23) Cacheris, W. P.; Nickle, S. K.; Sherry, A. D. *Inorg. Chem.* **1987**, *26*, 958.

notwithstanding. We thus studied two sets of mixed metal $Eu_{5-x}Ln_x$ samples: one in which the heteroatom is smaller (Ln = Tb) than europium and another where the heteroatom is larger (Ln = La). The higher energy peak (578.3 nm) in the spectrum of $Eu_{0.70}Tb_{4.30}$ (Figure 7a, insert spectrum C) corresponds to the major $Eu^{3+}(^5D_0) \rightarrow Eu^{3+}(^7F_0)$ emission while the major $Eu^{3+}(^5D_0) \rightarrow Eu^{3+}(^7F_0)$ emission of Eu_3La_2 is at ca. 579 nm (Figure 7a, insert-spectrum B). From the study of Chapell et al.[24] the $Eu^{3+}(^5D_0) \leftrightarrow Eu^{3+}(^7F_0)$ transition of $[Eu\mathbf{L}]^-$ species can be expected to be near 578 nm. We assign the peak at ca.578 nm in the emission and excitation spectra of polycrystalline $Eu_{5-x}Ln_x$ (Figure 7) to $Eu^{3+}(^5D_0) \leftrightarrow Eu^{3+}(^7F_0)$ transitions at **Site 1**; the low energy one (579 nm) is assigned to $Eu^{3+}(^5D_0) \leftrightarrow Eu^{3+}(^7F_0)$ transitions at **Site 2**. We conclude that for Eu_3La_2 the smaller Eu^{3+} ions are predominantly in **Site 2** while for compound $Eu_{0.70}Tb_{4.30}$ the now larger europium(III) ions are predominantly in **Site 1**. However, besides the possibility of energy transfer among europium(III) **Sites 1** and **Site 2**, site occupancy restrictions may not be entirely perfect since a shoulder is present at higher energy (ca. 578 nm) in the emission spectrum of Eu_3La_2 (indicating occupancy of **Site 1** by some Eu^{3+} ions) and at lower energy (ca. 579 nm) for $Eu_{0.70}Tb_{4.30}$ (indicating occupancy of **Site 2** by some Eu^{3+} ions). We conclude that during the formation of $Eu_{5-x}Ln_x$ hetero-pentanuclear nanoclusters, smaller lanthanide(III) ions are preferentially directed to coordination environments of **Site 2** while occupancy of **Site 1** by larger lanthanide(III) ions is preferable. Further evidence for the preference of **Site 1** by the larger lanthanide(III) ion is found in the FAB MS of the $Eu_{1.60}Dy_{3.40}$ complex in which the peak area of the $[EuH_2\mathbf{L}]^+$ ion is about 1.5 times that of $[DyH_2\mathbf{L}]^+$ compared to a much smaller value of about 0.5 expected from random occupancy of **Site 1** by both $[EuH_2\mathbf{L}]^+$ and $[DyH_2\mathbf{L}]^+$ ions. It was therefore interesting to study in detail the luminescence decay dynamical behavior of $Eu_{5-x}Ln_x$ crystals to determine whether energy transport within and between **Site 1** and **Site 2** locations can shed further light on the cooperative chemical and electronic activities involving hetero- and homo-pentanuclar nanoclusters.

Luminescence Decay Rates of Site 1 and Site 2 in $Eu_{5-x}Ln_x$; (Ln = Eu, Gd, La) Nanoclusters. Direct excitation of $Eu^{3+}(^5D_0)$ in **Site 1** and **Site 2** was readily achieved using a dye laser tuned at 578 and 579 nm, respectively. In both cases decay curves were obtained by monitoring the intense emission at 616 nm because of the poor spectral resolution of emission from the two sites in this region. The resulting decay curves are thus not expected to provide detailed information about individual **Site 1** or **Site 2** emission because of spectral overlaps, but information on major events such as energy migration or large differences in decay rates can be reliably extracted from the decay curves. Excitation (77 K) of the $Eu^{3+}(^5D_0)$ state in **Site 1** (λ_{exc} = 578 nm) of a largely gadolinium(III) complex containing a small amount of Eu^{3+} dopants, $Gd_{4.75}Eu_{0.25}$, results in an excitation build up with a rate of ca. 1.4×10^6 s^{-1} and a perfectly single exponential (for over five lifetimes) slow component decaying at 1.3×10^3 s^{-1} (Figure 8). Exciting **Site 2** at 77 K and 579 nm results in a fast component decaying at ca. 1.4×10^6 s^{-1} and a slow component (decay rate ca. 1.4×10^3 s^{-1}) of single-exponential behavior over five lifetimes. The "OH glue" in $Gd_{4.75}Eu_{0.25}$ is expected to quench $Eu^{3+}(^5D_0)$ emission of both **Site 1** and **Site 2** and its effect was not pursued because the products decompose in D_2O and are insoluble in other deuterated solvents.

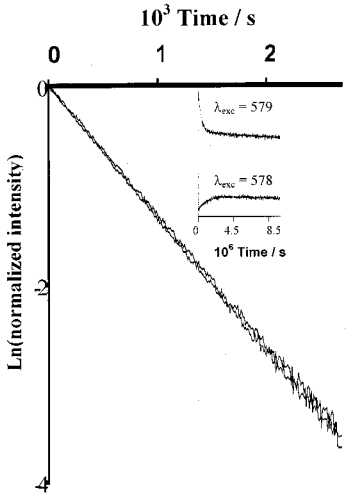

Figure 8. The similar 77 K decay curves of $Eu^{3+}(^5D0)$ in $Eu_{0.25}Gd_{4.75}$ for λ_{exc} = 579 and 578 nm (λ_{em} = 616 nm).

Within limits of the relatively low spectral resolution of **Site 1** and **Site 2** $Eu^{3+}(^5D_0)$ emission at 616 nm, we interpret these results as follows. We attribute the excitation build up observed when **Site 1** is excited to energy transfer from $Eu^{3+}(^5D_0)$ in **Site 1** to $Eu^{3+}(^5D_0)$ in **Site 2**. The quick component seen when **Site 2** is excited is due to quenching, probably by back energy transfer from $Eu^{3+}(^5D_0)$ in **Site 2** to $Eu^{3+}(^5D_0)$ in **Site 1**, because of the small thermal barrier (ca. 30 cm^{-1}). The very fast Eu^{3+}-$(^5D_0)$-to-$Eu^{3+}(^5D_0)$ energy transfer rate featured by $Gd_{4.75}Eu_{0.25}$ is likely to correspond to proximal Eu^{3+} ions in the same cluster, rather than between clusters (see next section). Since the sample is dilute in Eu^{3+} and f−f orbital overlaps are expected to be insignificant, it is reasonable to use the Dexter−Förster type[14] dipole−dipole interactions to assess Eu^{3+}−Eu^{3+} electronic interactions responsible for Eu^{3+}-to-Eu^{3+} energy transfer between **Site 1** and **Site 2**. These interactions should act across intracluster Eu−O−Eu bridges of 3.7−3.8 Å long (vide supra); the corresponding coupling constant is thus ca. 3.6×10^{-51} m^{6}s^{-1}. At 297 K the decay curves obtained by exciting at 578 and 579 nm are complex with the fast and single-exponential slow components decaying at ca. $3-4 \times 10^3$ and 1.5×10^3 s^{-1} respectively. There are weakly thermally activated quenching processes for $Eu^{3+}(^5D_0)$ in both **Site 1** and **Site 2**. To check these possibilities we studied the behavior of europium rich compounds Eu_3La_2 and Eu_5. Excitations of compound Eu_3La_2 at 77 K and 578 nm produces perfectly single-exponential and temperature independent luminescence decay kinetics with a rate of ca.1.5×10^3 s^{-1}. We conclude that energy migration (among similar $Eu^{3+}(^5D_0)$ sites of either **Site 1** or **Site 2**) and transfer (between $Eu^{3+}(^5D_0)$ states of **Site 1** and those of **Site 2**) are efficient enough to homogenize the entire $Eu^{3+}(^5D_0)$ population in the complex. Indeed, direct excitation (λ_{exc} = 578 and 579 nm) of the homopentanuclear europium(III) complex Eu_5 also reveals perfectly single exponential and temperature independent decay behavior of the $Eu^{3+}(^5D_0)$ emission with a rate of ca. 1.5×10^3 s^{-1}. Since the emission and excitation spectra of Eu_5 (Figure 7) confirmed luminescence activity from two $Eu^{3+}(^5D_0)$ environments complete homogenization of those environments, which results in a dynamic energy transport regime characterized by perfectly single-exponential luminescence decay kinetics, [25] must be effected by fast energy migration and transfer over the entire $Eu^{3+}(^5D_0)$ population. The efficiency of this energy migration/transfer behavior, which

(24) Chappell, L. L.; Voss, D. A. V.; Horrocks, W. D., Jr.; Morrow, J. R. *Inorg. Chem.* **1998**, *37*, 3989.

(25) Huber, D. L. *Phys. Rev. B* **1979**, *20*, 2307 and 5333.

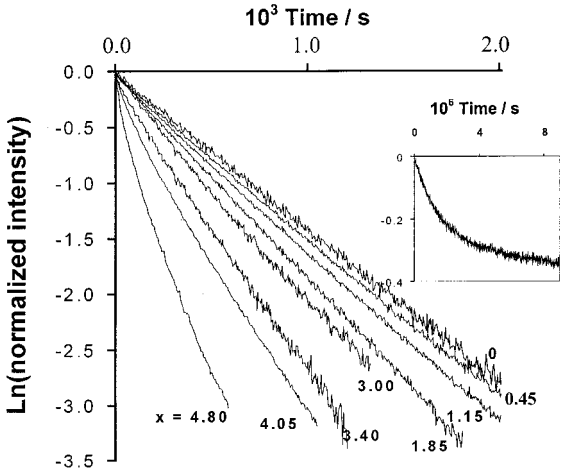

Figure 9. The 77 K decay profiles for $Eu^{3+}(^5D_0)$ in $Eu_{5-x}Dy_x$(λ_{exc} = 578 nm, λ_{em} = 616 nm). The insert shows the fast-decaying component for $Eu_{3.85}Dy_{1.15}$.

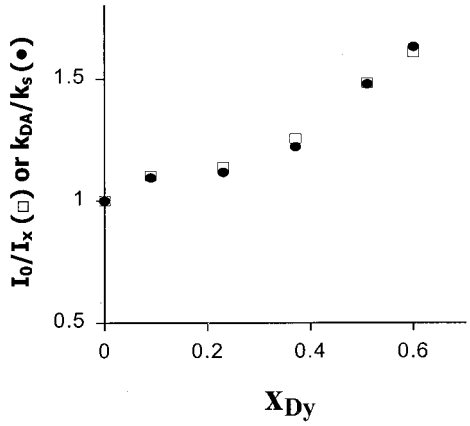

Figure 10. 77 K Stern−Volmer plots (ratios of decay rates, kDA/ks (●), and intensities, I_o/I_x (□), against the mole fraction of Dy^{3+} (x_{Dy}) for Eu^{3+} ($^5D_0$) emission in $Eu_{5-x}Dy_x$ complexes. I_0 and I_x are the normalized integrated intensity for long-lived Eu^{3+} ($^5D_0$) emission in the absence and presence of Dy^{3+}, respectively; k_{DA} = decay rate of $Eu^{3+}(^5D_0)$ in the presence of Dy^{3+}; k_s = decay rate of Eu^{3+} ($^5D_0$) in Eu_5.

reflects the single-entity-like behavior of the clusters, was studied in more detail using the hetero-lanthanide(III) complexes $Eu_{5-x}Ln_x$ (Ln = Sm and Dy) where the Sm^{3+} and Dy^{3+} are known to be relatively slow and fast quenchers of $Eu^{3+}(^5D_0)$ emission, respectively. [8,13c,19]

Energy Transport among Ln^{3+} ions in $Eu_{5-x}Ln_x$ (Ln = Sm, Dy) Nanoclusters. Direct excitation (λ_{exc} = 578 or 579 nm) of $Eu^{3+}(^5D_0)$ in polycrystalline $Eu_{5-x}Dy_x$ ($x < 3.5$) complexes, yields quenched long-lived emission, which exhibits single-exponential behavior at 297 K (see Supporting Information). The decay curves feature weak temperature dependence and deviate rather marginally from single-exponential behavior at 77 K, especially at high Dy^{3+} concentrations (Figure 9). There is also a short-lived component of (decay rate, ca. 9×10^5 s^{-1} at 77 K) (Figure 9 insert). With much higher dysprosium concentrations, e.g., in $Eu_{5-x}Dy_x$ (x = 4.05 and 4.8), the curves become complicated which is consistent with reduced energy migration due to the low concentration of Eu^{3+} sites and the resulting multiplicity of possible europium−dysprosium couplings. Possible Eu−O−Dy distances range from 3.7 to 3.8 Å (for Ln-Ln linkages with multiple Ln−O−Ln bridges, i.e., Ln(1)−Ln(2), Ln(1)−Ln(2A), Ln(1)−Ln(3), Ln(2)−Ln(3), Ln(1A)−Ln(3), and Ln(2A)−Ln(3)) to 5.5 Å (for C_2 symmetry related positions Ln(2)−Ln(2A) and Ln(1)−Ln(1A)). Quenching of the long-lived $Eu^{3+}(^5D_0)$ emission by Dy^{3+} in $Eu_{5-x}Dy_x$ ($x \leq 3$) follows Stern−Völmer[26] kinetics with a limiting rate of ca. 4.4×10^3 s^{-1} which is similar to the limiting decay rate (ca. 3×10^3 s^{-1}) derived from the slow component of emission from $Eu_{0.20}Dy_{4.8}$ crystals. Stern−Völmer plots employing decay rates and normalized integrated intensities against the concentration of Dy^{3+} are coincident (Figure 10) indicating that energy transport in $Eu_{5-x}Dy_x$ crystals is diffusive.[26] We attribute the limiting rate of the slow component ($k_{inter} = 4.4 \times 10^3$ s^{-1}) to relatively inefficient direct-*inter*nanocluster (shortest separation R ≈ 9.33 Å) europium-to-dysprosium energy transfer, which is much slower than intercluster $Eu^{3+}(^5D_0)$-to-$Eu^{3+}(^5D_0)$ energy migration. For internanocluster europium-to-dysprosium energy transfer which involves long metal−metal separations, through-space Dexter−Förster type dipole−dipole interactions are expected to dominant; we obtain a corresponding europium−dysprosium coupling constant $C \approx 6.4 \times 10^{-52}$ m^6s^{-1}. This simple two-body intercluster europium−dysprosium dipole−dipole coupling constant is of comparable magnitude to the one that is active across phenolate Eu−O−Dy bridges of dinuclear complexes ($C \approx 7 \times 10^{-52}$ m^6s^{-1}). [8,13c,19] However, such simple two-body mechanisms breakdown for intrananocluster (shortest Eu−Dy separation is ca. 3.7 Å) europium-to-dysprosium energy transfer. Accordingly, a simple two-body dipole−dipole energy transfer rate estimated from the Dexter−Förster mechanism is $k_{EuDy} \approx 3 \times 10^5$ s^{-1}, which is significantly slower than the experimental value of ca. 10^6 s^{-1} derived from the fast component of emission from dysprosium rich polycrystalline systems such as Eu_2Dy_3. While this short emission is significant in understanding the nature of $Dy^{3+}-Eu^{3+}$ interactions, the emission decayed too quickly to study in detail with our setup. We thus turned to the $Eu_{5-x}Sm_x$ complexes because the samarium(III)−europium(III) coupling constant across Sm−O−Eu bridges is known to be roughly 1/20 that of the corresponding dysprosium(III)−europium(III) couple;[8,13c,19] hence quenching of $Eu^{3+}(^5D_0)$ within individual $Eu_{5-x}Sm_x$ ($0 < x < 5$) nanoclusters is expected to be slower and more readily measurable compared to that of the $Dy^{3+}-Eu^{3+}$ couples in similar environments.

The decay curves of $Eu_{5-x}Sm_{x)}$ ($x < 3.5$) (monitored at 616 nm) following direct excitation of $Eu^{3+}(^5D_0)$ at 578 nm and 77 or 297 K are very complicated in the early part (Figure 11); the long-time components are marginally quenched and single-exponential. The decay curves are intermediate between dynamic and static limits. Stern−Volmer plots, obtained using normalized integrated luminescence intensities of the complex early-time parts of the decay curves, provide direct intracluster europium-to-samarium energy transfer rates of ca. 7.4×10^3 (at 77 K) and 1.0×10^4 (at 297 K) s^{-1}. The temperature dependence of the energy transfer rate is due to the participation of $Sm^{3+}(^6H_{7/2})$ level, which is expected to be significantly populated at 297 K (Boltzman's population of the $Sm^{3+}(^6H_{7/2})$ state relative to that of the ground-state $Sm^{3+}(^6H_{5/2})$ is ca. 0.007). These limiting decay rate estimates of the major emission are of the same order of magnitude as the value of ca. 1.1×10^4 s^{-1} predicted using the Dexter−Förster relationship in the dipole−dipole mode and a coupling constant of ca. 2.9×10^{-53} m^6s^{-1} exhibited by Eu−O−Sm phenolate bridges of dinuclear complexes.[8] Since the relative ionic size difference between Eu^{3+} (0.950 Å) and Sm^{3+} (0.964 Å) is not too large, it is reasonable to expect some randomness in the partition of both of these cations between

(26) Stern, O.; Volmer, M. *Z. Physik* **1919**, *20*, 183. Demas, J. N. *Excited-State Lifetime Measurements*; Academic Press: New York, 1983.

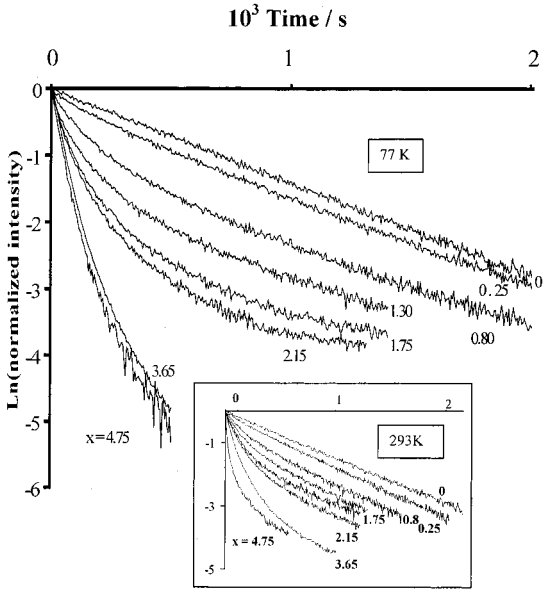

Figure 11. The 77 K decay profiles for $Eu^{3+}(^5D_0)$ in $Eu_{5-x}Sm_x$ (λ_{exc} = 578 nm, λ_{em} = 616 nm). The insert shows the corresponding 293 K decay profiles. The decay curves cover 0−2 ms for both temperatures.

Site 1 and **Site 2**. Thus, the multiplicity of $Eu^{3+}(^5D_0)$ environments in polycrystalline $Eu_{5-x}Sm_x$ should have origin in the large differences in possible Eu−O−Sm distances (i.e., 3.7−3.8 Å and 5.50 Å as discussed above for Eu−O−Dy bridges). Corresponding two-body europium-to-samarium energy transfer rates facilitated by dipole−dipole interactions across these Eu−O−Sm bridges are expected to be 1.2×10^4 and 1.0×10^3 s^{-1}. Complex luminescence decay curves are thus expected, unless the $Eu^{3+}(^5D_0)$-to-$Eu^{3+}(^5D_0)$ interclusters energy migration rate is much faster than 1.2×10^4 s^{-1}. The observed intermediate energy transport behavior means that energy migration among $Eu^{3+}(^5D_0)$ sites is not efficient enough to homogenize the population of $Eu^{3+}(^5D_0)$ excited states in the various $Eu_{5-x}Sm_x$ ($0 < x < 5$) nanoclusters present in the polycrystalline samarium(III)−europium(III) complexes (Figure 11).

It is noteworthy that decay curves of samples very rich in samarium, such as $Eu_{5-x}Sm_x$ (x = 3.65 and 4.75), exhibit unusually fast decay rates (ca. 1×10^5 s^{-1} for the short-lived component and ca. 3×10^4 s^{-1} for the long-lived one). These dramatically fast decay rates, are much larger than the rate (at most ca. 1.2×10^4 s^{-1}) expected from a simple two-body $Sm^{3+}-Eu^{3+}$ dipole−dipole interaction across Sm−O−Eu bridges. Thus for samples concentrated in samarium(III), simple two-body energy transfer mechanisms also break down; dominant processes appear to be more consistent with new and more efficient europium-to-samarium energy transfer mediated by multiple samarium(III) ions. We propose that when excited $Eu^{3+}(^5D_0)$ states are surrounded by many $Sm^{3+}(^6H_{5/2})$ species (as in the nanocluster $EuSm_4$, cooperative quenching mechanisms arising from electronic coupling between one $Eu^{3+}(^5D_0)$ and several $Sm^{3+}(^6H_{5/2})$ states become active. For example, a near resonant three-body energy transfer process involving the most intense emission band ($Eu^{3+}(^5D_0) \rightarrow Eu^{3+}(^7F_2)$) and two Sm^{3+} ions is plausible for a $EuSm_4$ cluster:

$$2Sm^{3+}(^6H_{5/2}) + Eu^{3+}(^5D_0) \rightarrow Eu^{3+}(^7F_2) + 2Sm^{3+}(^6F_{7/2}) \quad (3)$$

Similar cooperative three-body processes can be advanced to explain the unexpectedly fast decay rate (ca. 1×10^6 s^{-1}) of $Eu^{3+}(^5D_0)$ emission in the $Dy^{3+}-Eu^{3+}$ couples of samples rich in Dy^{3+} (see also a higher slope in the Stern−Völmer plot in Figure 10) such as Eu_2Dy_3:

$$2Dy^{3+}(^6H_{15/2}) + Eu^{3+}(^5D_0) \rightarrow Eu^{3+}(^7F_2) + 2(Dy^{3+}(^6H_{9/2}) \text{ and/or } Dy^{3+}(^6F_{11/2})) \quad (4)$$

Because of the multiplicity of the $Eu^{3+}(^5F_J)$ as well as the ^6H_J and ^6F_J states[29] of Sm^{3+} and Dy^{3+} many three-body combinations with potential for cooperative action can be envisaged. Many-body luminescence-quenching mechanisms[27] may be particularly important when the $Eu^{3+}(^5D_0)$ species is in positions similar to those occupied by Nd3 in Figure 1 from which short simultaneous contacts with four potential Dy^{3+} or Sm^{3+} emission quenchers are possible.

Concluding Remarks

In conclusion, crystals of hetero-lanthanide(III) complexes $Ln'_{5-x}Ln_x$ are built from a variety of molecular pentanuclear lanthanide(III) $Ln'_{5-x}Ln_x$ ($x = 0-5$) nanoclusters. Clearly, small Ln^{3+} ions have large ionic potentials than larger Ln^{3+} ions. During the activities of molecular recognition processes which assemble the hetero-lanthanide(III) pentanuclear nanoclusters, complementarity between $[Ln\mathbf{L}]^-$ and $[(Ln(NO_3)_2]^+)$ components directs large Ln^{3+} ions to **Site 1** (as $[Ln\mathbf{L}]^-$), which provides better Lewis base character for the alkoxide sites, while smaller Ln^{3+} ions are directed to **Site 2** (to serve as bridging $[Ln(NO_3)_2]^+$). In this profound expression of complementarity[28] Lewis acid−base interactions between the acidic Ln^{3+} coordination sites of $[Ln(NO_3)_2]^+$ and the basic alkoxide sites of $[Ln\mathbf{L}]^-$ are maximized as is required for optimal stability of hetero-lanthanide nanoclusters. Promiscuous population of a few **Site 1** and **Site 2** positions by smaller and larger Ln^{3+} ions, respectively, is probably a consequence of the high thermodynamic and kinetic stability of $[Ln\mathbf{L}]^-$ ions[20] which may slow the rates at which "coordination errors can be corrected". Luminescence studies revealed extensive metal−metal electronic coupling within and between nanoclusters including the possibility of many-body processes. The energy transport regime in crystalline $Eu_{5-x}Ln_x$ ($x = 0$ and Ln = La, $x = 2$) complexes is in the dynamic limit and involves $Eu^{3+}(^5D_0)$ in both **Site 1** and **Site 2**. In the context of energy transfer, the nanoclusters in the pure europium, mixed europium−lanthanum, and europium−dysprosium compounds at 293 K are essentially behaving as single-entities. With $Eu_{5-x}Ln_x$ (Ln = Sm and Dy) complexes the energy transport regime at 77 K (and at 293 K for europium−samarium compounds) is intermediate between the dynamic and static limits because intracluster $Eu^{3+}-Sm^{3+}$ and $Eu^{3+}-Dy^{3+}$ energy transfer processes are, in these cases, efficient. The unusually fast $Eu^{3+}-Sm^{3+}$ and $Eu^{3+}-Dy^{3+}$ energy transfer rates are consistent with the single entity behavior in which many-body processes are active. In such processes, one $Eu^{3+}(^5D_0)$ state may be electronically coupled to several Sm^{3+} or Dy^{3+} ions which may cooperatively quench its emission, particularly at high samarium or dysprosium concentrations. Conversely, many-body processes may also be

(27) Bettinelli, M. In *Vibronic Processes in Inorganic Chemistry*; Flint, C. D., Ed.; Kluwer: Dordrecht, 1989; p 347.
(28) Lehn, J.-M. *Supramolecular Chemistry, Concepts and Perspectives*; VCH: Weiheim, 1995; p 11. Cram, D. J.; Cram, J. M. Container Molecules and their guests. *Monographs in Supramolecular Chemistry*; Stoddart, J. F., Ed.; Royal Society of Chemistry: Cambridge, 1994; p 39.
(29) Dieke, G. H. *Spectra and Energy Levels of Rare Earth Ions in Crystals*; Crosswhite, H. M., Crosswhite, H., Eds.; Interscience: New York, 1968; p 142.

possible at low samarium or dysprosium concentrations because two $Eu^{3+}(^5D_0)$ states may electronically couple to one Sm^{3+} or Dy^{3+} ion and enable it to achieve high excitation energies while they ($Eu^{3+}(^5D_0)$) simultaneously relax to lower energy levels. Many-body processes in $Ln'_{5-x}Ln_x$ ($x = 1-4$) nanoclusters are possible because of the "μ_5-OH^-" glue that links all the five Ln^{3+} ions in the pentanuclear nanocluster and of course, further interactions are possible through the alkoxide Ln′−O−Ln bridges. Three-body processes are known but not well understood.[27] Suitable, new materials with capacity for sensitized $Eu^{3+}(^5D_0)$ emission, which can then facilitate investigations at high energy acceptor concentrations, are being sought for studies on such many-body energy transfer processes.

Acknowledgment. We thank the Inter-American Development Bank-UWI development program for funding (R&D project # 29), the UWI for a scholarship to M.K.T. and a Research and Publications Grant, Prof. S. V. Ley and Dr. P. Grice of Cambridge University for assistance with mass spectra, and Prof. Gerald C. Lalor, Director General, International Centre for Environmental and Nuclear Sciences for supporting the work and helpful discussions.

Supporting Information Available: The 293 K decay profiles for $Eu^{3+}(^5D_0)$ in $Eu_{5-x}Dy_x$ ($\lambda_{exc} = 578$ nm, $\lambda_{em} = 616$ nm). This material is available free of charge via the Internet at http://pubs.acs.org.

IC0102440